# Chapter 6 – Experimental results

## 6.1 Diodes before irradiation

Several diodes for each processed wafer were characterised before irradiation by C-V, I-V and charge collection measurements. This allows the choice, for each type of material, of sets of diodes with similar characteristic. In total, almost one hundred detectors were selected, irradiated and measured.

Significant differences have been noticed between planar and mesa devices fabricated from the same material.

The reverse current at full depletion of a mesa diode is in the order of µA and for a planar is in the order of nA. The difference is certainly due to the charge injected by the edge of the detector, which are more damaged in mesa diodes. Mesa diodes exhibit also a shorter minority carrier lifetime, which has been measured by the reverse recovery (RR) method: ≈ 15 µs for mesa's and ≥ 70 µs for planar's.

Differences between the charge collection properties of mesa and planar detectors are explained by the thickness of the diffused junction and ohmic contact.

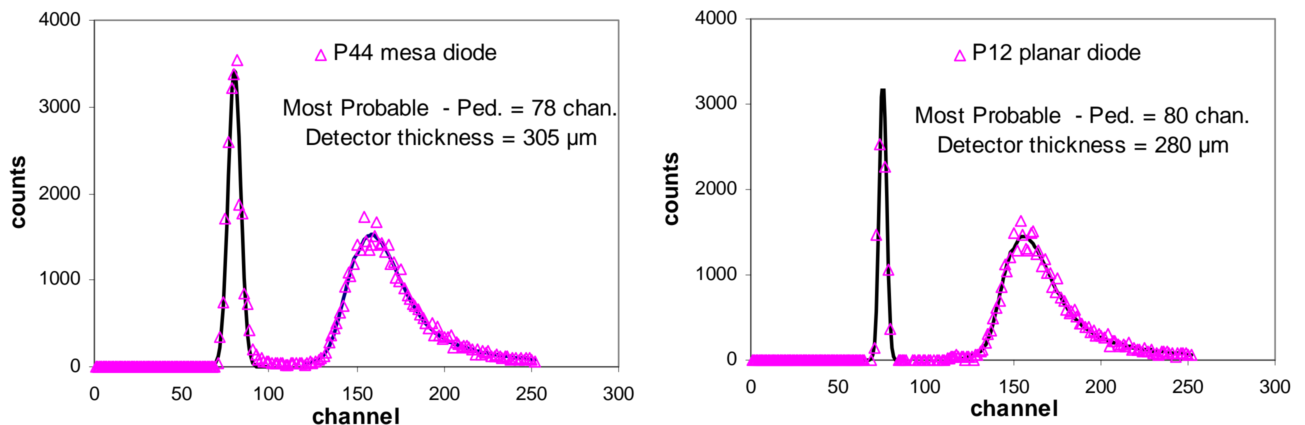


Fig. 6.1 *Energy spectra, recorded by an ADC, of $\beta^-$ particles from $^{106}$Ru in overdepleted (a) mesa and (b) planar diodes.*

The highly doped $p^+$ and $n^+$ regions do not deplete (or, better, they deplete very little) in a reverse biased diode, so they are non-sensitive to the passage of an ionising particle. Figure 6.1 shows the energy spectra of 2 MeV electrons (Minimum Ionising Particles) from a $^{106}$Ru source for mesa and planar diodes biased above their full depletion voltage ($V_{FD}$ + 10 volts). The difference between the most probable value of the Landau distribution and the pedestal is proportional to the length of the particle path inside the detector. The electron trajectories have been collimated perpendicularly to the detector surface, so that this difference is proportional to the detector active thickness. For the 280 µm thick planar diode and for the 305 µm thick mesa diode, the measured most-probable values are 80 and 78 channels, respectively. The junction and the ohmic contact thickness for planar diodes is < 1 µm and the energy lost in this non-sensitive layers is neglected. Assuming the same charge collection efficiency (CCE) per unit length for these non-irradiated diodes, the dead layer of the mesa detector is deduced to be ≈ 28 µm. This dead layer is the sum of the junction and the ohmic contact depths, which are evaluated ≈ 14 µm each.

The Van de Graaf accelerator of Prague [6.1] provided protons with tuneable energy up to 2.5 MeV. The maximum range of these protons in silicon is ≈ 70 µm. Figure 6.2 shows the energy of the impinging protons versus the ADC channel corresponding to the maximum charge collected by non-irradiated planar and mesa detectors illuminated through the junction side.

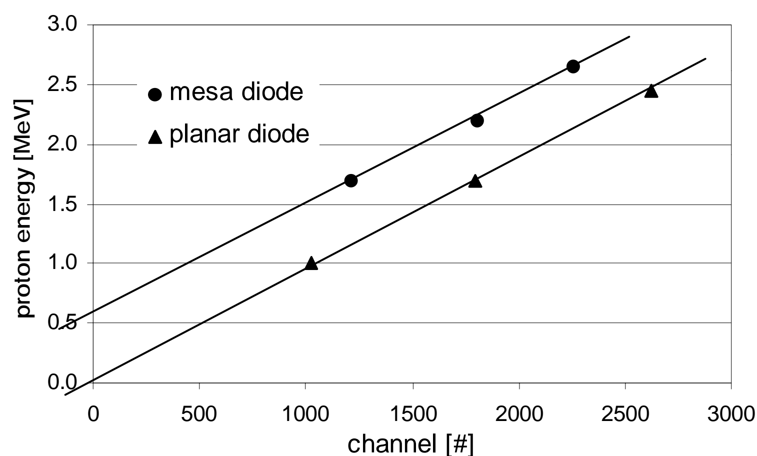


Fig. 6.2 *Energy of impinging protons versus ADC channel for mesa and planar non irradiated diodes.*

The intersection of the linear fit for the planar detector with the axis of energy is ≈ 0.1 MeV, while it is ≈ 0.6 MeV for the mesa diode. This indicates that a proton loses ≈ 0.5 MeV before entering the sensitive part of a mesa diode. Assuming, in a first approximation, that low-range protons with energies ≥ 1.7 MeV loose the same amount of energy in the first part of their path in silicon, the energy loss of 0.5 MeV corresponds to a depth of ≈ 18-20 μm.
As a consequence of these results, the effective thickness of mesa diode is ≈ 25 μm less than the geometrical thickness.

## 6.2 Proton irradiations

The proton irradiations have been performed in the CERN-PST7 proton beam, with proton momentum of 24 GeV/c.
$N_{eff}$ was obtained from $V_{FD}$ measured with the C-V method. The I-V characteristics were measured together with the C-V and the values of the reverse current at full depletion were used for the calculation of $I_{vol}$. The study of a specific type of detectors as a function of the fluence can be performed in two different ways.
Each sample of a set of similar detectors is irradiated up to a different fluence and the changes of the electrical properties are obtained by measuring the complete set. Alternatively, one sample is irradiated up to the maximum fluence by successive step of intermediate fluences and measured after each step. The first technique requires a large amount of samples. The measurements presented here have been performed using the second technique.

### 6.2.1 $N_{eff}$ as a function of the fluence

$N_{eff}$ depends on the time after irradiation. The rate of the beneficial annealing is faster immediately after irradiation. Fast components of annealing have been found [6.2] in the case of neutron irradiation. It is necessary to know the annealing rate to compare $N_{eff}$ results of different diodes irradiated and measured on various time scales. In the case of proton, the irradiations take place over a relatively long time (compared to the typical time of the faster component of the annealing), and the proton flux depends on the number of spills available

from the PS supercycle. The flux can change between different irradiations and the detectors of different runs could be in a different annealing stage at the end of the irradiation. The correction parameters to retrieve the value of $N_{eff}$ at the end of the irradiation are not available. The estimate of a set of parameters for the correction algorithm requires the experimental measurement of the evolution of $N_{eff}$ with time on irradiated samples, at a given temperature and with a negligible irradiation time. The last condition cannot be met for proton irradiations. Therefore no correction for the short term annealing of $N_{eff}$ is applied, but the samples to be compared are irradiated under the same conditions and together with a reference sample, whose known behaviour allows the normalisation of the results between different runs of irradiations. All the diodes were measured in a short delay (1.5 – 2 hours) after the end of each irradiation step.

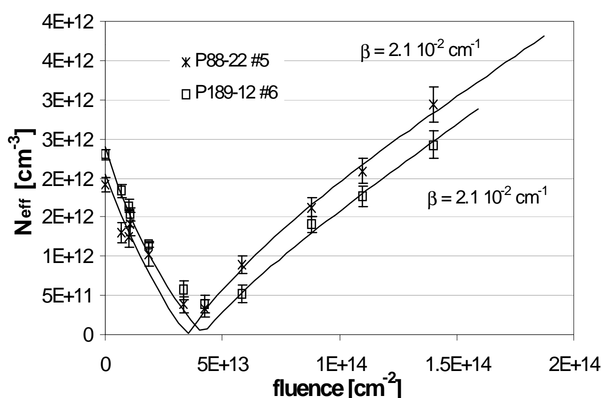


Fig. 6.3 *$N_{eff}$ versus fluence for standard (#5) and weakly oxygenated (#6) diodes processed by SINTEF.*

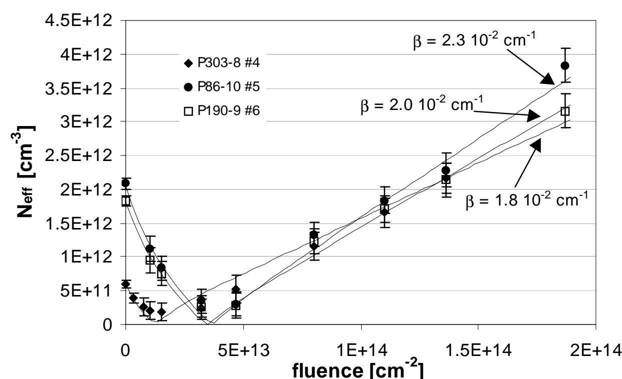


Fig. 6.4 *$N_{eff}$ versus fluence for standard (#4, #5) and weakly oxygenated (#6) diodes. #4 is processed by ITE,* #5 and #6 by SINTEF.

Figure 6.3 shows $N_{eff}$ as a function of fluence for planar diodes from standard (#5 of Table 5.3) and weakly oxygenated (#6) silicon. The type inversion fluence is ≈ 17 times the value of the effective doping concentration before irradiation, $N_{eff}(0)$. The value of the $\beta$ constant, which describes the introduction rate of acceptor-like defects (eq. 3.13), is $(2.1 \pm 0.3) \cdot 10^{-2}$ cm$^{-1}$ for both types of diodes (irradiation in April '97). Figure 6.4 shows $N_{eff}$ as a function of the fluence for planar diodes made from high resistivity standard silicon (#4 an #5) and from weakly

oxygenated silicon (#6) (irradiation in June '97). The type inversion fluence is respectively ≈ 21, ≈ 17 and ≈ 18 times $N_{eff}(0)$. $\beta$ is (1.8 ± 0.3) $\cdot 10^{-2}$ cm $^{-1}$, (2 ± 0.3)$\cdot 10^{-2}$ cm $^{-1}$ and (2.3 ± 0.3)$\cdot 10^{-2}$ cm$^{-1}$ respectively.

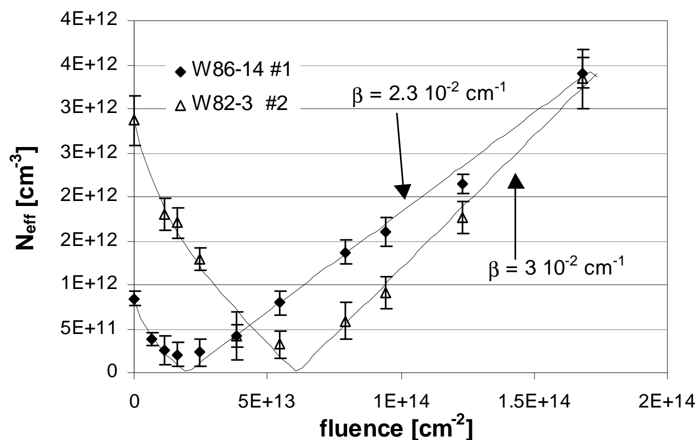


Fig. 6.5 *$N_{eff}$ versus fluence for standard diodes with a different starting resistivity.*

Figure 6.5 shows the comparison between two planar diodes made by CANBERRA from standard silicon of different resistivity (#1 and #2). The type inversion fluence is about 20$\cdot N_{eff}(0)$. The value of the $\beta$ constant is (2.3 ± 0.3)$\cdot 10^{-2}$ cm$^{-1}$ and (3.0 ± 0.3) $\cdot 10^{-2}$ cm$^{-1}$ for the higher and the lower resistivity respectively (irradiation in July '97).

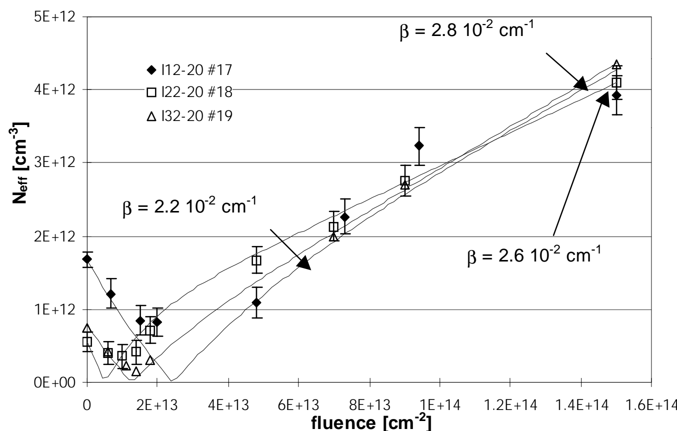


Fig. 6.6 *$N_{eff}$ versus fluence for epitaxial planar n-type diodes (#17, #18, #19).*

Figure 6.6 shows $N_{eff}$ as a function of fluence for planar epitaxial n-type diodes (#17, #18, #19). The thickness of the epitaxial layer is 100, 150 and 200 μm and the corresponding type

inversion fluences are ≈ 17, ≈ 12 and ≈ 20·$N_{eff}$ *(0)*. The low value of the type inversion fluence for the 150 μm thick wafer is due to a poor quality of the fit because of the few points measured before inversion for this high resistivity material. $\beta$ is (2.2 ± 0.3)·$10^{-2}$, (2.6 ± 0.3)·$10^{-2}$ and (2.8 ± 0.3)·$10^{-2}$ cm $^{-1}$ for the 100, 150 and 200 μm respectively.

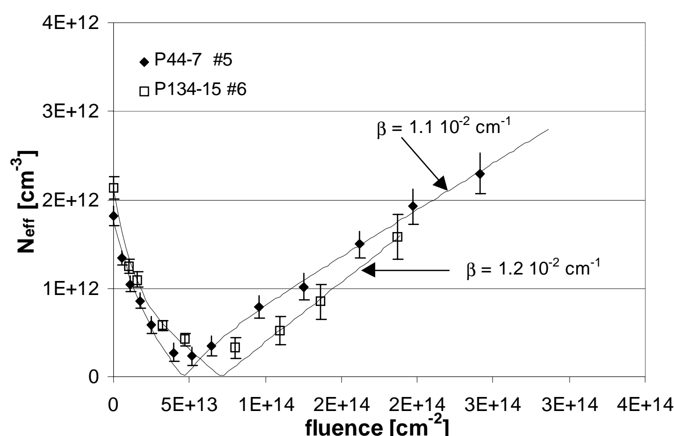


Fig. 6.7 *$N_{eff}$ versus fluence for mesa standard (#5) and weakly oxygenated diodes (#6).*

Figure 6.7 shows a similar plot for mesa diodes manufactured by DIOTEC from standard and weakly oxygenated materials (#5, #6). The type inversion fluence is ≈ 27·$N_{eff}$ *(0)* for the standard and ≈ 32·$N_{eff}$ *(0)* for the oxygenated silicon. $\beta$'s are (1.1 ± 0.3)·$10^{-2}$ cm$^{-1}$ and (1.2 ± 0.3)·$10^{-2}$ cm$^{-1}$ for standard and oxygenated, respectively. These mesa diodes are processed from the same materials as the planar diodes of Figures 6.3 and 6.4.

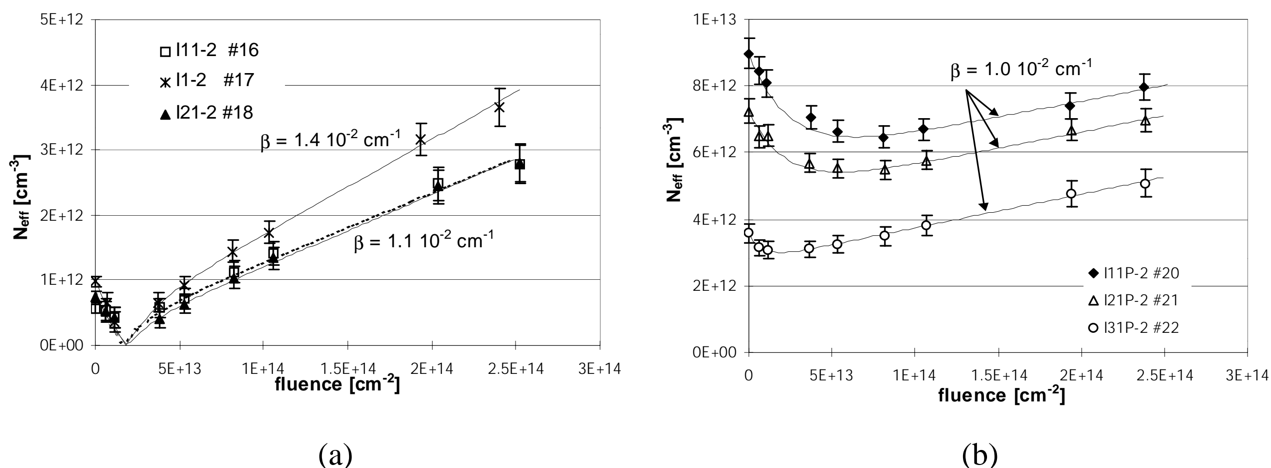


(a) (b)

Fig. 6.8 *$N_{eff}$ versus fluence for mesa epitaxial (a) n-type and (b) p-type diodes.*

Figure 6.8 shows $N_{eff}$ versus fluence for mesa diodes manufactured by DIOTEC on various epitaxial silicon wafers (from #16 to #22). The type inversion fluences for the n-type diodes (Fig. 6.8(a)) are between 20 to 30 times $N_{eff}(0)$, but the accuracy of the estimate is poor because of the few points available about inversion. P-type diodes (Fig. 6.8(b)) do not invert their conductivity type but undergo a strong decrease of $N_{eff}$ at low fluence. The values of $\beta$'s are between $(1.1 \pm 0.3)\cdot 10^{-2}$ and $(1.4 \pm 0.3)\cdot 10^{-2}$ cm$^{-1}$ for n-type materials and $\approx (1.0 \pm 0.3)\cdot 10^{-2}$ cm$^{-1}$ for p-type materials. The n-type materials are similar to the ones used for manufacturing the planar diodes shown in Fig 6.6. Figures 6.9 exhibit a comparison between a typical planar and mesa diode made from similar FZ and epitaxial materials.
The parameters extracted from the experimental data are summarised in Table 6.1.

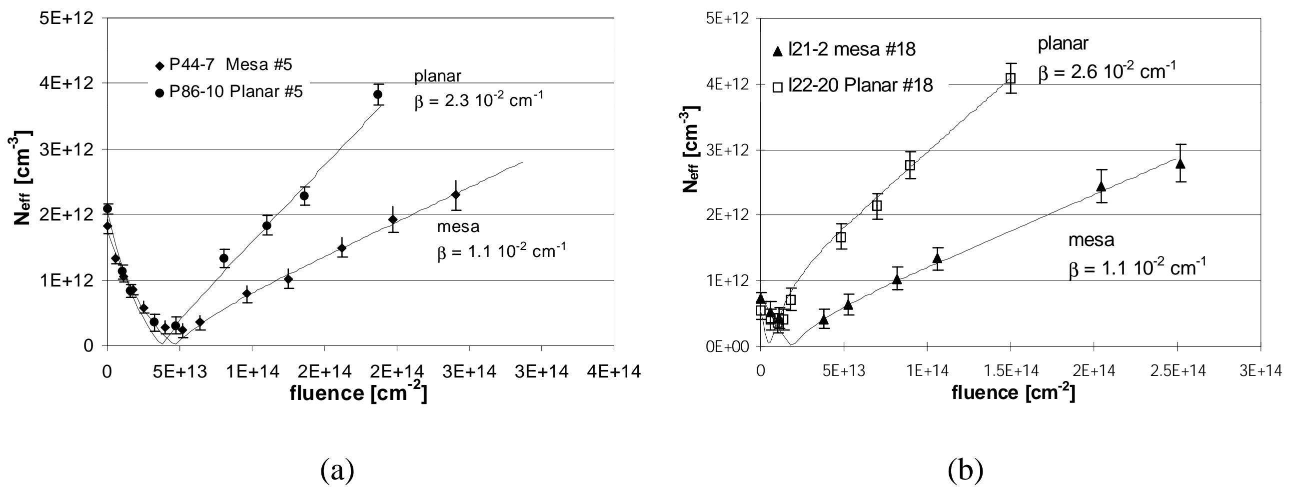


(a) (b)

Fig. 6.9 *Comparison of $N_{eff}$ versus fluence between planar and mesa diodes: (a) standard FZ and (b) epitaxial diodes.*

### 6.2.2 $N_{eff}$ as a function of the time after irradiation

The long term behaviour of the irradiated detectors has been studied storing them at room temperature until the end of the beneficial annealing and then accelerating the annealing rate by heating stages at 80 °C. The time is expressed in equivalent days at room temperature, using eq. 3.16. The fit to the experimental data is performed using eq. 3.14 and the amplitude of the reverse annealing, $g_y$, is calculated from eq. 3.15.

Figures 6.10 (a) and (b) show $N_{eff}$ as a function of the time after irradiation for planar and mesa detectors irradiated in April '97 to $1.1 \cdot 10^{14}$ and $1.8 \cdot 10^{14}$ $cm^{-2}$. The diodes are made from standard (#5) and weakly oxygenated silicon (#6). The value of the $g_y$ constant ranges from 2.8 to 3.5 ± 0.4 $10^{-2}$ $cm^{-1}$ for the planar diodes and is 2.3 ± 0.4 $10^{-2}$ $cm^{-1}$ for the mesa one. Figure 6.10 (b) evidences the beneficial annealing phase, which takes place over ≈ 10 days at room temperature.

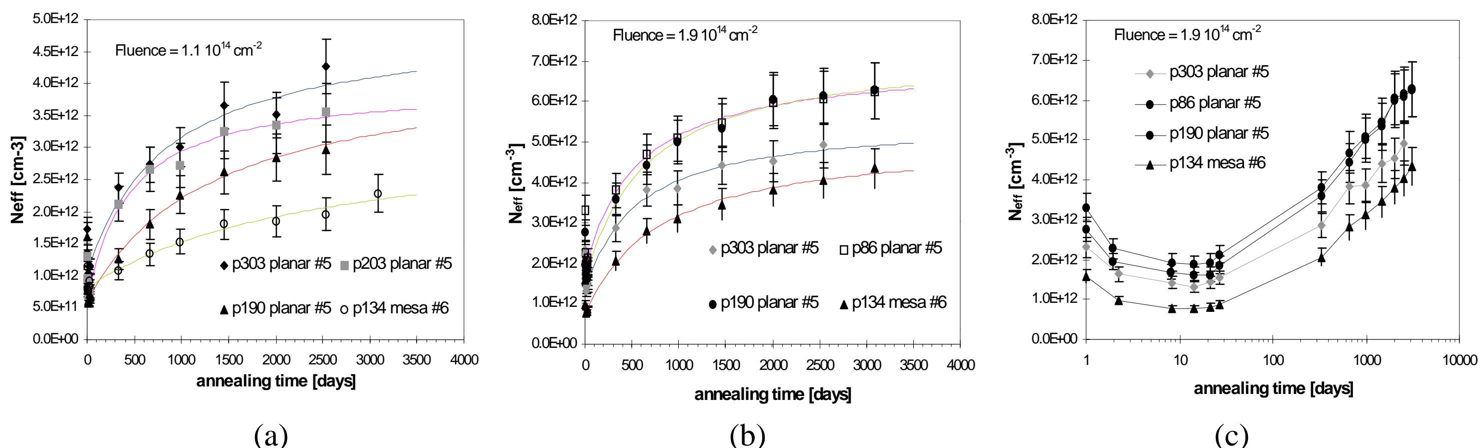


Fig. 6.10 $N_{eff}$ *versus annealing time (room temperature equivalent) for planar and mesa diodes made from materials #5 and #6 and for two different final fluences: (a) $1.1 \cdot 10^{14}$ $cm^{-2}$, (b) $1.9 \cdot 10^{14}$ $cm^{-2}$. Picture (c) is the same as (b)but plotted in logarithmic scale to evidence the beneficial annealing (irradiation April '97).*

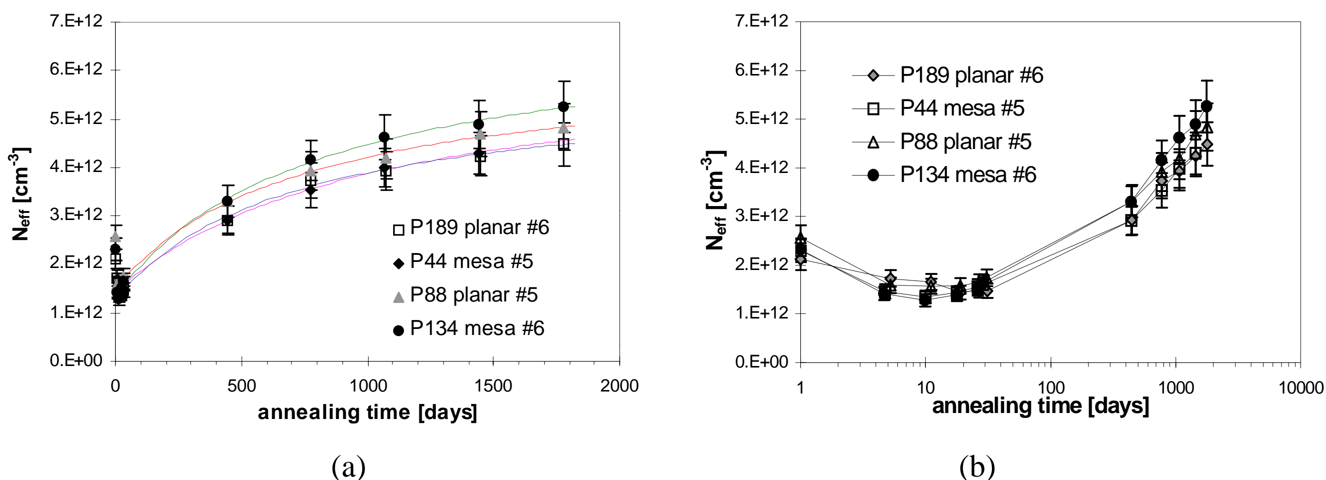


Fig. 6.11 $N_{eff}$ *versus annealing time (room temperature equivalent) for planar and mesa diodes made from materials #5 and #6. The final fluence is $1.4 \cdot 10^{14}$ $cm^{-2}$. The plot (b) in logarithmic scale evidences the beneficial annealing (irradiation June '97).*

Figure 6.11 shows $N_{eff}$ as a function of the time after irradiation for planar and mesa detectors irradiated in June '97 to $1.4 \cdot 10^{14}$ $cm^{-2}$. The diodes are made from standard (#5) and weakly oxygenated (#6) silicon. $g_y$' ranges from 3.0 to 3.5 ± 0.4 $10^{-2}$ $cm^{-1}$ for planar diodes and is ≈ 2.1 ± 0.4 $10^{-2}$ $cm^{-1}$ for the mesa ones. The plot in logarithmic scale shows a phase of slow changes in the $N_{eff}$ values between 10 to 50 days at room temperature.

Figure 6.12 shows similar plots for planar and mesa detectors made from epitaxial silicon (#16 to #19) irradiated in August '97 to $1.8 \cdot 10^{14}$ $cm^{-2}$. $g_y$ ranges from 4.4 to 6.0 ± 0.4 $10^{-2}$ $cm^{-1}$ for the planar diodes and from 3.0 to 3.8 ± 0.4 $10^{-2}$ $cm^{-1}$ for the mesa ones.

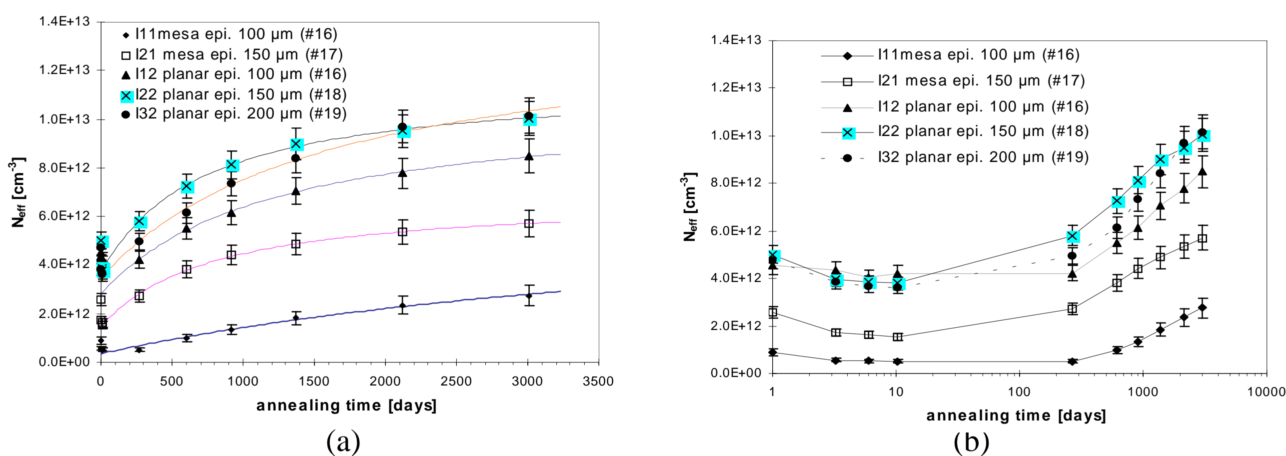


Fig. 6.12 *$N_{eff}$ versus annealing time (20 °C equivalent) for planar and mesa diodes made from epitaxial materials (#17 to #19). The final fluence is $1.8 \cdot 10^{14}$ $cm^{-2}$. The plot (b) in logarithmic scale evidences the beneficial annealing (irradiation August '97).*

The values of the parameters obtained from the data for the various materials are summarised in Table 6.1.

### 6.2.3 Reverse current as a function of the fluence

The volume currents are measured at full depletion, normalised to room temperature (20 °C) using eq. 3.10 and corrected for the annealing using eq. 3.11, unless otherwise specified.Figure 6.13 shows the reverse volume current as a function of fluence for planar diodes made from standard silicon of high and low resistivities (#1 and #2). The value of the damage constant

$\alpha$ is $(4.5 \pm 0.3)\cdot 10^{-17}$ A cm$^{-1}$. The current was measured with the guard-ring not connected, therefore the error depends on the fluence: the reverse current for both diodes is very close for the lowest values of the fluence, and diverge substantially when the fluence increases. As described in § 4.2, only the values of the current at low fluences have been included into the fitting points. This procedure has been followed for all the measurements performed with floating G-R.

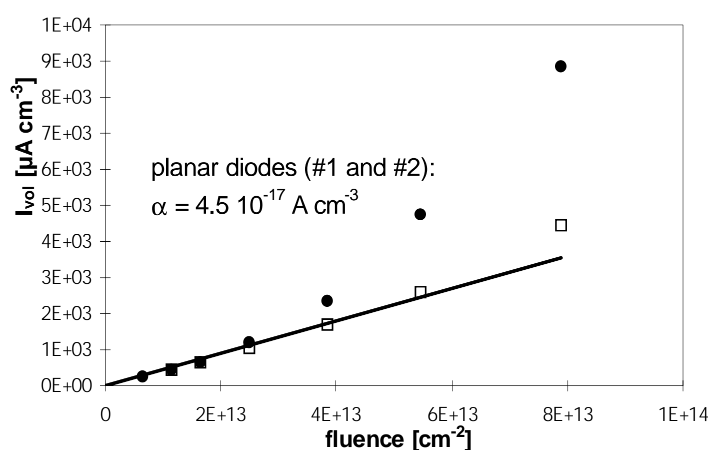


Fig. 6.13 *Reverse leakage current versus fluence for planar diodes made from standard materials with different resistivities (#1 and #2).*

Figure 6.14 shows the volume reverse current as a function of the fluence for planar diodes processed by ITE and SINTEF from standard low and high resistivity (#4 and #5) and weakly oxygenated (#6) silicon. The fits give $\alpha = (5.0 \pm 0.3)\cdot 10^{-17}$ A cm$^{-1}$ for all the diodes. Figure 6.15 shows a similar plot for CANBERRA planar diodes made from epitaxial silicon (# 17, #18 and #19). The value of $\alpha$ is $(4.8 \pm 0.3)\cdot 10^{-17}$ A cm$^{-1}$.

The reverse current changes in mesa diodes can not be related to the volume generation current. Figure 6.17 shows the reverse current versus fluence for three mesa diodes from the same wafer. The behaviours do not follow the expectation. The high current before irradiation depends mostly on extra-bulk components. The large difference between the three diodes also indicates the influence of the process, probably the sawing and the passivation steps, on the reverse current of a particular sample. It is therefore not possible to compare the reverse current

changes between planar and mesa diodes by the direct measurement of the current at full depletion.

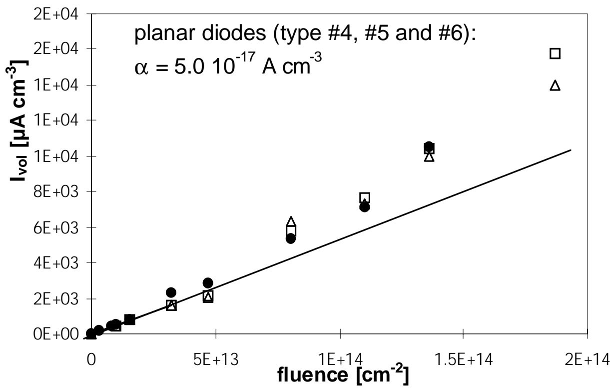


Fig. 6.14 *$I_{vol}$ versus fluence for planar diodes made from FZ materials #4, #5 and #6.*

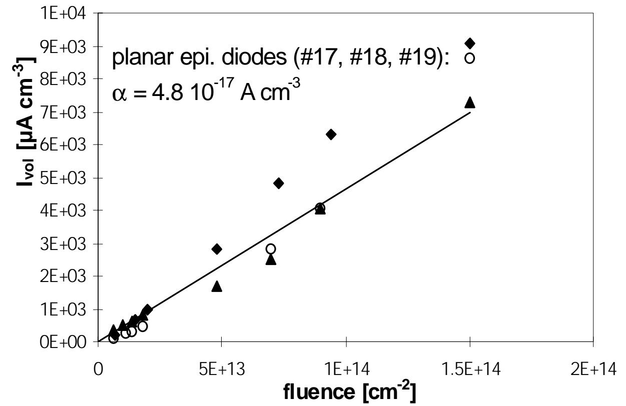


Fig. 6.15 *$I_{vol}$ versus fluence for planar diodes made from epitaxial materials #17, #18 and #19.*

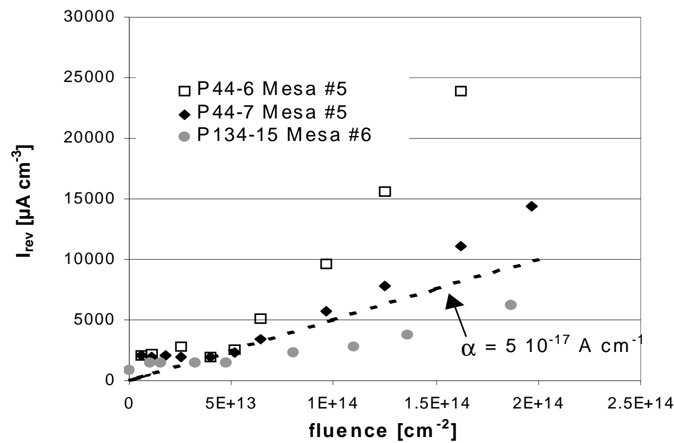


Fig. 6.16 *$I_{vol}$ versus fluence for mesa diodes from the same standard silicon wafer (#5) and from a weakly oxygenated wafer (#6).*

## 6.3 Neutron irradiations

The neutron irradiations have been performed at the Triga research nuclear reactor of the Jozef Stefan Institute of Ljubljana, Slovenia. This facility allows very high fluxes, up to $10^{13}$ $cm^{-2}$ $s^{-1}$. The typical irradiation time is ≈ 10-15 minutes. About ten minutes more are required, after

irradiation, to achieve a low radioactivity before handling the diodes. In this situation the time needed for a measurement is comparable to the fast component of the annealing and a large error is introduced by the delay between successive measurements of $N_{eff}$ and $I_{vol}$.

The comparison between different materials was performed irradiating and measuring all the samples under investigation in the same conditions. Alternatively, the annealing technique was used. The idea of this latter method is to speed up the beneficial annealing heating the detectors at 80 °C after irradiation, in order to reach the bottom part of the annealing curve. The rate of change of $N_{eff}$ after the end of the beneficial annealing is very slow, and the error due to $N_{eff}$ or $I_{vol}$ measurements performed at a different time after the end of the irradiation is negligible. Figure 6.17 shows $V_{FD}$ as a function of the time at 80 °C for non-inverted n-type diodes. The almost stable value corresponding to the end of beneficial annealing is achieved after ≈ 3 minutes.

Figure 6.18 shows the difference of $N_{eff}$ between three pairs of similar detectors irradiated up to $1 \cdot 10^{14}$ cm$^{-2}$. One sample of each pair was successively irradiated and heated for 4 minutes at 80 °C in seven steps of intermediate fluences ($1.0 \cdot 10^{13}$, $1.5 \cdot 10^{13}$, $2.5 \cdot 10^{13}$, $4.0 \cdot 10^{13}$, $6.0 \cdot 10^{13}$, $8.0 \cdot 10^{13}$, $1.0 \cdot 10^{14}$ cm$^{-2}$). At the end of the irradiations, the radiation defects induced by the first step of $1.0 \cdot 10^{13}$ cm$^{-2}$ have sustained 7 annealing steps, while the defects induced by the last irradiation step sustained only one annealing. The other sample of the pair was irradiated directly to $1 \cdot 10^{14}$ cm$^{-2}$ and annealed once during 4 minutes at the same temperature. The difference between the $N_{eff}$ values obtained from the single and the multiple annealing stages is less than 10%.

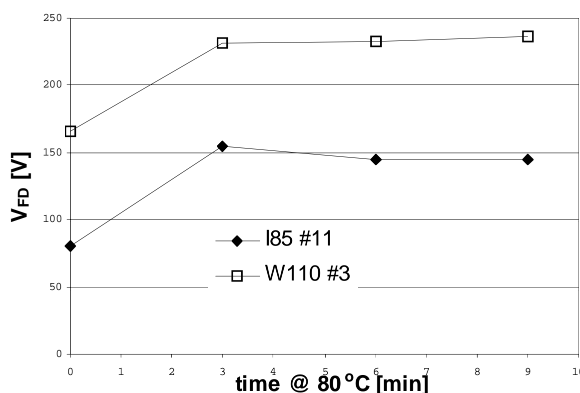


Fig. 6.17 *$V_{FD}$ versus time at 80 °C for non-inverted standard (#3) and jet oxygenated (#11) diodes after irradiation.*

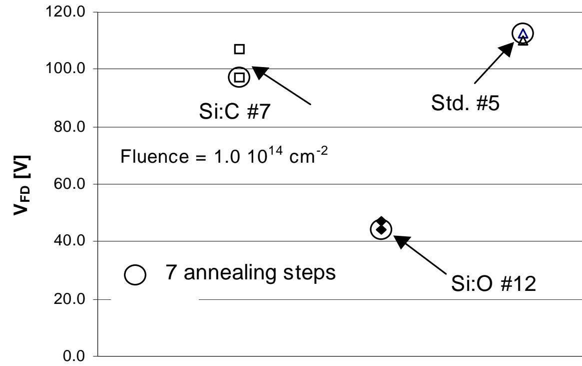


Fig.6.18 C*omparison between $V_{FD}$ measured after a fluence of $1{\cdot}10^{14}$ $cm^{-2}$ for three pairs of diodes either submitted successively to 7 irradiations and annealing steps (circled points) or irradiated directly to the final fluence and annealed in one step only. Each annealing step is 4 min. at 80 °C.*

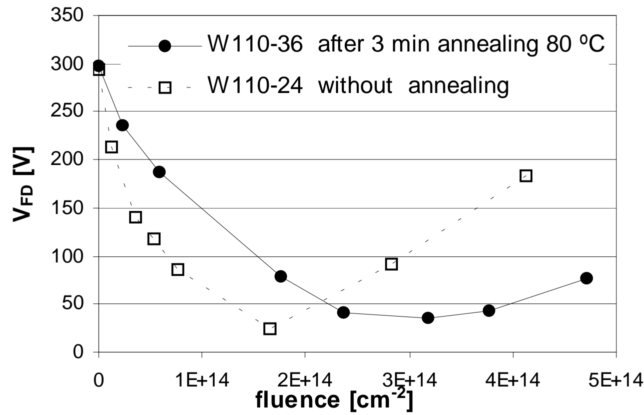


Fig. 6.19 *Comparison between $V_{FD}$ as a function of the fluence measured ≈ 30 min. after irradiation and at the end of the beneficial annealing for two similar detectors.*

Figure 6.19 shows the comparison between $V_{FD}$ measured after the annealing during three minutes at 80 °C after each irradiation step or ≈ 30 minutes after irradiation for two similar detectors irradiated with neutrons. $N_{eff}$ increases with the annealing time for fluences below the type inversion and, inversely, decreases for fluences above the type inversion. The change of $N_{eff}$ is smaller and the type inversion fluence is noticeably higher.

Both methods have been used during the neutron irradiation. The relevant parameters of the radiation hardness behaviour ($\beta$, $\alpha$, type inversion fluence) are rather different. The subscript "*ann*" indicates below the parameters obtained from annealed diodes.

### 6.3.1 $N_{eff}$ as a function of the fluence

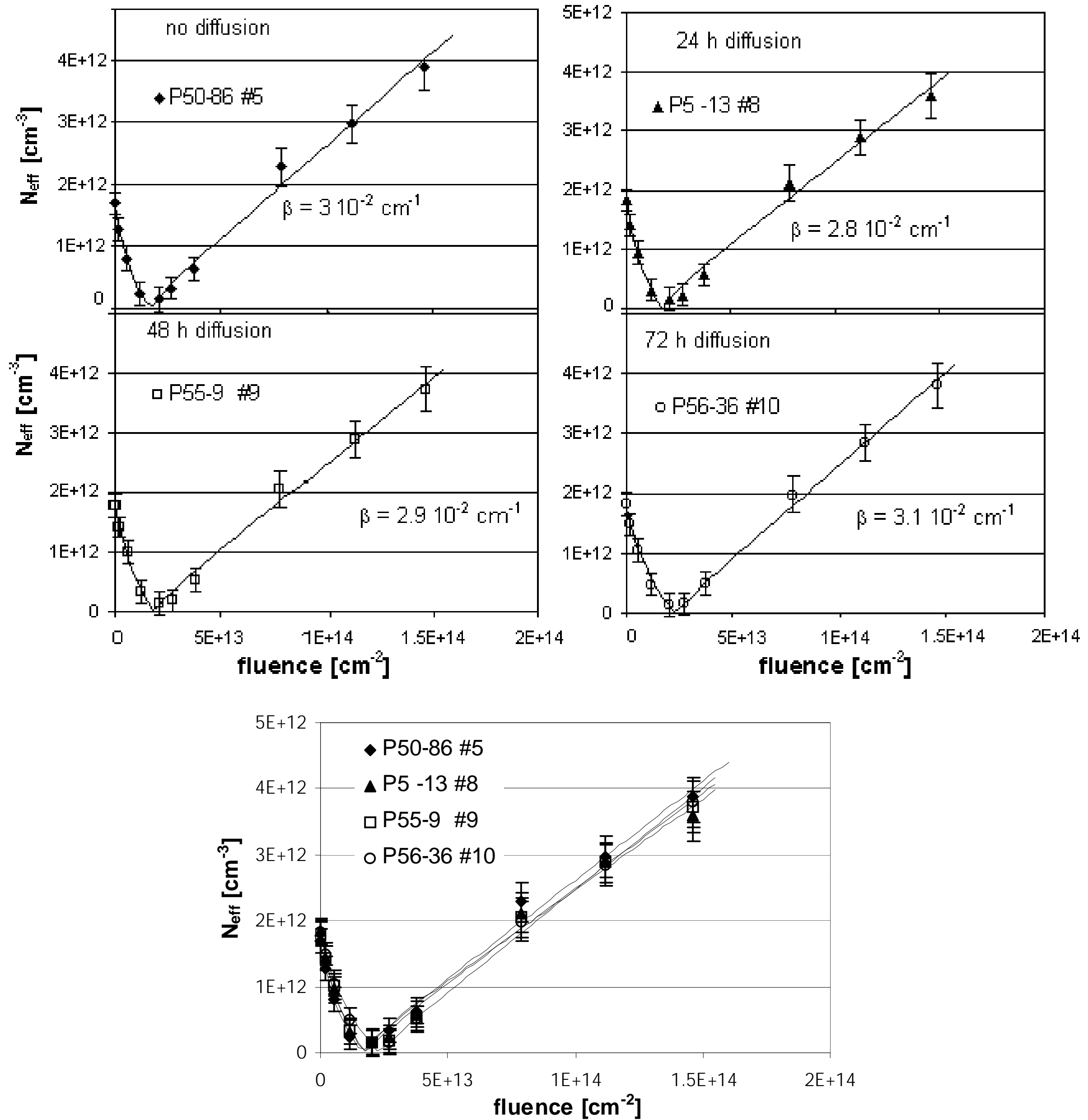


Fig. 6.20 *$N_{eff}$ versus fluence for planar diodes made from standard (#5) and O-diffused (#8, #9 and #10) silicon. The diffusion time of oxygen at 1150 °C is indicated in the pictures.*

Figure 6.20 shows $N_{eff}$ as a function of the fluence for planar diodes made from standard (#5) and O-diffused (#8, #9 and #10) silicon materials. The type inversion fluence is ≈ $10 \cdot N_{eff}(0)$ and $\beta$ is ≈ $3 \cdot 10^{-2}$ cm$^{-1}$ for each of them.

Figure 6.21 shows $N_{eff}$ as a function of the fluence for planar diodes made from MACOM epitaxial material 150 μm thick (#15). The type inversion fluence is ≈ $9 \cdot N_{eff}(0)$ and $\beta$ is equal to $(2.5 \pm 0.3) \cdot 10^{-2}$ cm$^{-1}$.

Figure 6.22 shows a comparison between an epitaxial (#15) and a planar oxygen diffused detector #9).

Fig. 6.23 shows a comparison between a standard (#5) and NTD detectors (#23 and #24).

The data presented above were obtained by measuring the detectors irradiated in the same conditions and measured after a delay of 30-60 minutes after irradiation.

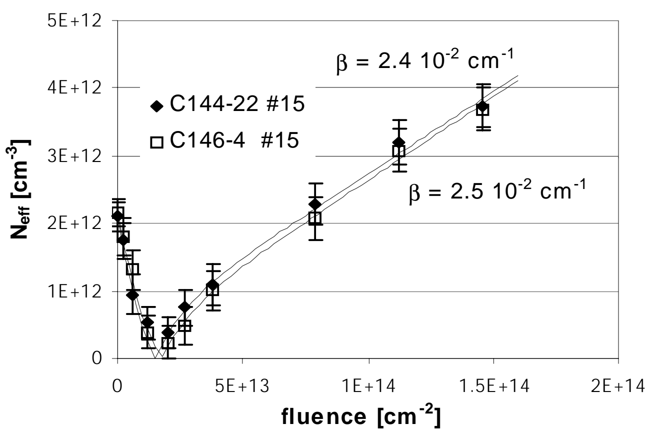


Fig. 6.21 *$N_{eff}$ versus fluence for planar diodes made from epitaxial materials (#15).*

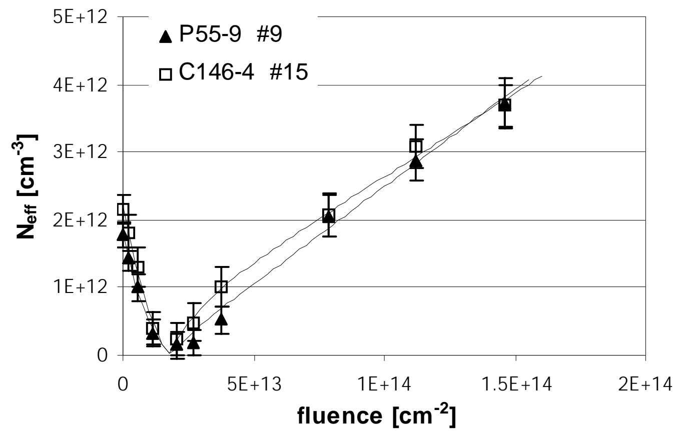


Fig. 6.22 Comparison of *$N_{eff}$ versus fluence for planar diodes made from O diffused FZ (#9) and epitaxial materials (#15).*

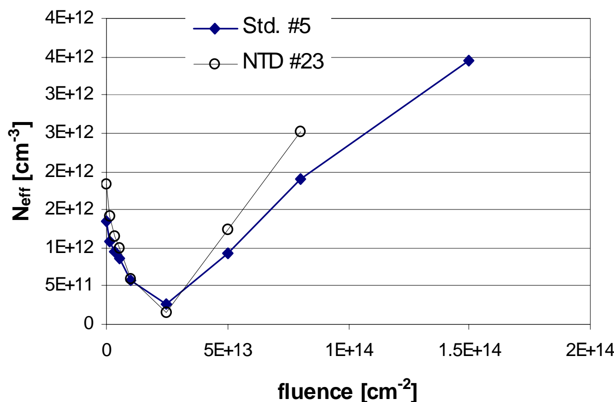


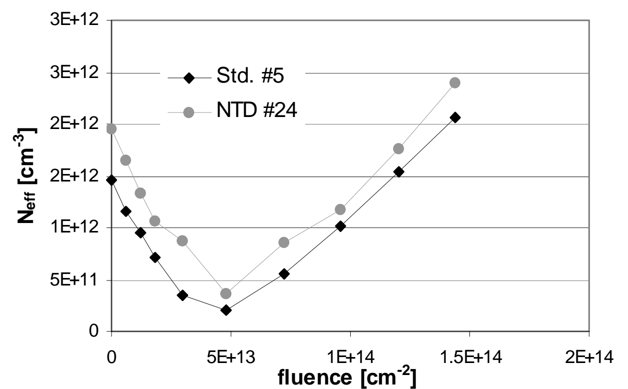


Fig 6.23 *Comparison of $N_{eff}$ versus fluence between standard (#5) and NTD diodes (#23, #24).*

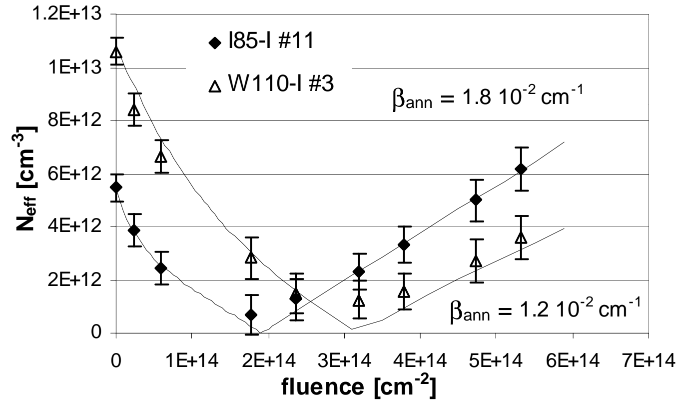


Fig. 6.24 *$N_{eff}$ versus fluence for planar diodes made from FZ low resistivity standard (#3) and jet oxygenated (#11) silicon.*

The following results have been obtained using the annealing method.

Figure 6.24 shows $N_{eff}$ as a function of the fluence for planar ITE diodes made from jet oxygenated (#11) and standard low resistivity FZ silicon (#3). $\beta_{ann}$ is (1.8 ± 0.3) $\cdot 10^{-2}$ cm$^{-1}$ for the oxygenated and (1.2 ± 0.3) $\cdot 10^{-2}$ cm$^{-1}$ for the standard materials. The type inversion fluence is ≈ $30 \cdot N_{eff}(0)$ and ≈ $34 \cdot N_{eff}(0)$ for the standard and the oxygenated materials, respectively.

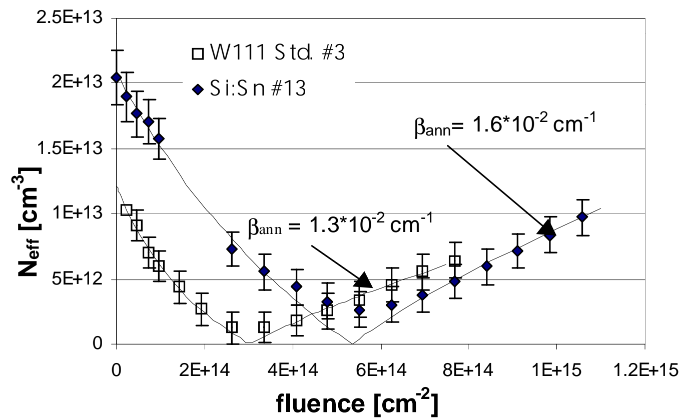


Fig 6.25 *$N_{eff}$ versus fluence for planar diodes made standard low resistivity silicon #3 and tin enriched low resistivity silicon #13.*

Figure 6.25 shows $N_{eff}$ as a function of fluence for planar diodes made from Sn-enriched (#13) and standard low resistivity (#3) silicon. $\beta_{ann}$ is (1.6 ± 0.3)$\cdot 10^{-2}$ cm$^{-1}$ and (1.3 ± 0.3)$\cdot 10^{-2}$ cm$^{-1}$

for the Sn-enriched and the standard silicon, respectively, and the type-inversion fluence is ≈ $26 \cdot N_{eff}(0)$ for both materials.

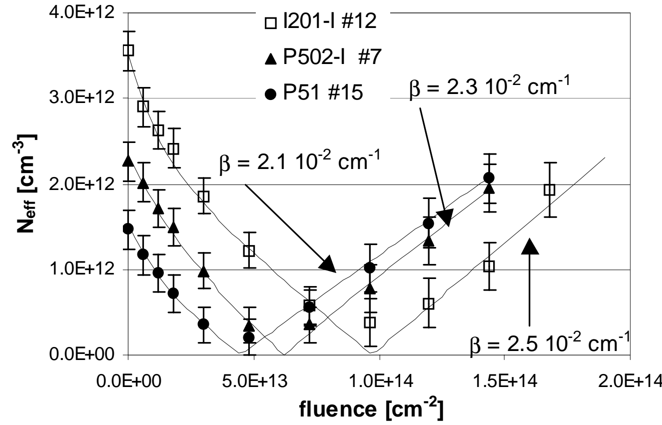


Fig. 6.26 *$N_{eff}$ as a function of the fluence for planar diodes made from standard (#5), carbonated (#7) and jet-oxygenated (#12) silicon.*

Figure 6.26 shows $N_{eff}$ as a function of the fluence for planar diodes made from standard (#5), carbonated (#7) and jet-oxygenated (#12) silicon. $\beta_{ann}$ is (2.0 ± 0.05), (2.3 ± 0.05) and (2.5 ± 0.05)$\cdot 10^{-2}$ cm$^{-1}$ for the standard, carbonated and the jet-oxygenated, respectively. The type inversion fluence is ≈ $30 \cdot N_{eff}(0)$ for the standard and $27 \cdot N_{eff}(0)$ for carbonated and jet-oxygenated diodes.

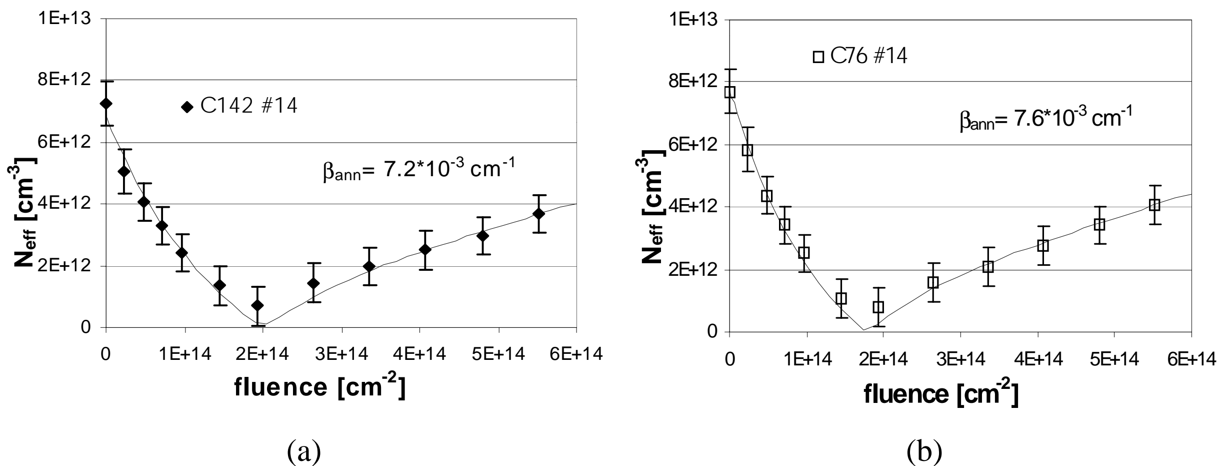


Fig. 6.27 *$N_{eff}$ versus fluence for planar diodes made from MACOM 100 µm epitaxial silicon #14 (a) 5x5 mm$^2$ square diode (b) 1.36 cm$^2$ round device.*

Figure 6.27 shows $N_{eff}$ as a function of the fluence for planar diodes made from similar MACOM 100 µm epitaxial wafers (#14). $\beta_{ann}$ is $(0.76 \pm 0.05)\cdot10^{-2}$ cm$^{-1}$ and $(0.72 \pm 0.05)\cdot10^{-2}$ cm$^{-1}$ for the two samples and the type inversion fluence is $\approx 22\cdot N_{eff}(0)$ for both diodes.

### 6.3.4 $N_{eff}$ as a function of the time after irradiation

.

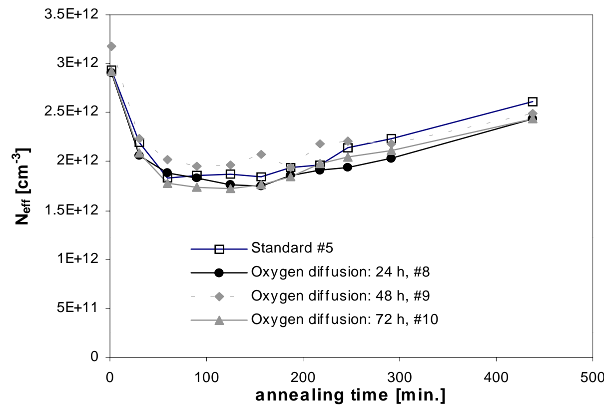


Fig. 6.28 *$N_{eff}$ as a function of the annealing time at 60 °C for planar diode made from standard (#5) and O-diffused (#8, #9 and #10) silicon. Irradiation fluence: $1.5\cdot10^{14}$ cm$^{-2}$.*

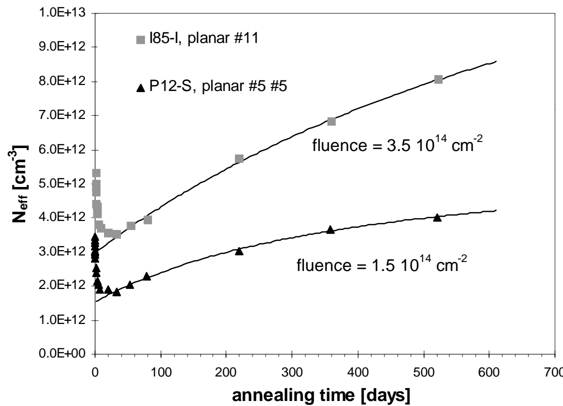


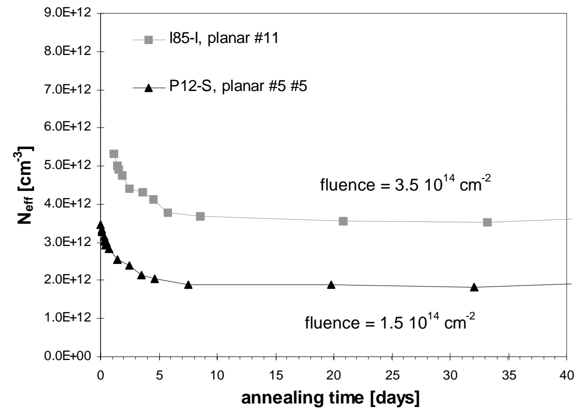


(a) (b)

Fig. 6.29 *$N_{eff}$ as a function of the time after irradiation for planar and mesa diode made from standard material (#5) and planar diodes made from jet-oxygenated silicon (#11): (a) full scale (b) limited scale to evidence the beneficial annealing.*

Figure 6.28 shows $N_{eff}$ as a function of the annealing time at 60 °C for standard (#5) and O-diffused materials (#8, #9 and #10). The diodes have been irradiated up to $1.5 \cdot 10^{14}$ $cm^{-2}$.

Figure 6.29 shows $N_{eff}$ as a function of the time after irradiation for planar diodes made from standard (#5) and jet-oxygenated silicon (#11). The fluence is 1.5 $10^{14}$ $cm^{-2}$ for the standard and 3.5$10^{14}$ $cm^{-2}$ for the jet-oxygenated diode. $g_y$ is (3.01 ± 0.4) $10^{-2}$ $cm^{-1}$ for the standard and (4.29 ± 0.4) $10^{-2}$ $cm^{-1}$ for the jet-oxygenated detector

### 6.3.3 Reverse current as a function of the fluence

Figure 6.30 shows the reverse current, measured without contacting the guard-ring, as a function of the fluence for a standard and an oxygen diffused planar diodes (#5 and #9) irradiated in February '98 and measured ≈ 30' after irradiation.

Together with these diodes were irradiated diodes made from oxygenated materials #7 and #10, which exhibit similar behaviours. $\alpha$'s values are ≈ 6.0 $\cdot 10^{-17}$ A $cm^{-1}$.

Figure 6.31 shows $I_{vol}$ as a function of the fluence for two diodes made from similar MACOM 150 μm epitaxial wafers (#15) irradiated in the same time as the previous samples. The value of $\alpha$ is $6.3 \cdot 10^{-17}$ and $6.7 \cdot 10^{-17}$ A $cm^{-1}$ for the two samples.

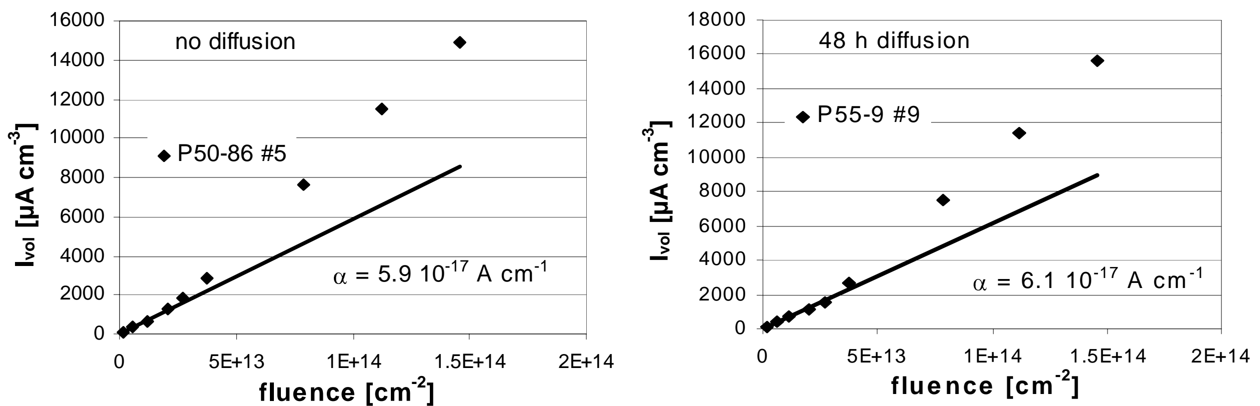


Fig. 6.30 *$I_{vol}$ as a function of fluence for planar diodes made from standard (#5) and oxygen diffused (#9) wafers.*

Figure 6.32 shows the reverse current as a function of the fluence for standard and tin-enriched planar diodes (#3 and #13) irradiated in June '98. The diodes have been annealed during 4 minutes at 80 °C before the measurement. $\alpha_{ann}$ is $(3.1 \pm 0.3)\cdot 10^{-17}$ A cm$^{-1}$ for the tin enriched and $(2.9 \pm 0.3)\cdot 10^{-17}$ A cm$^{-1}$ for the standard diode.

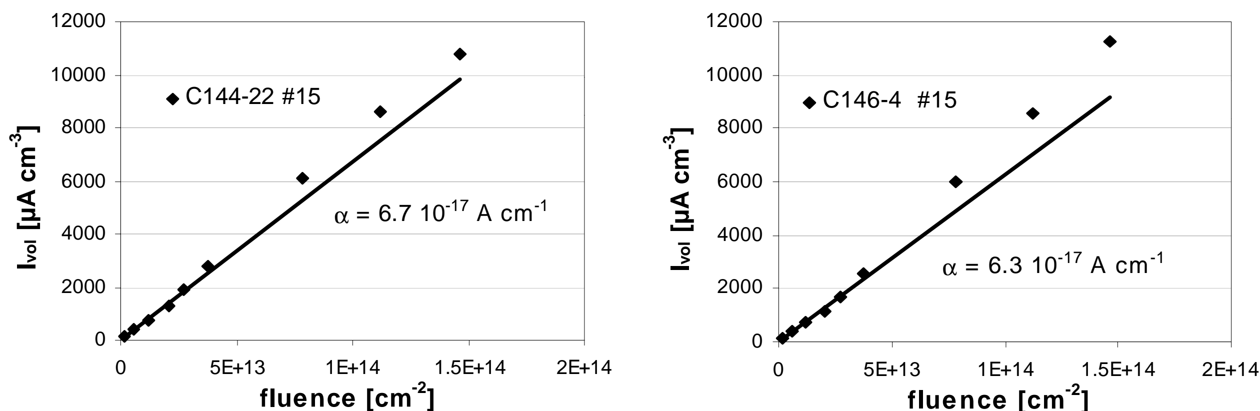


Fig. 6.31 *$I_{vol}$ as a function of fluence for planar diodes made from similar epitaxial wafers (#15).*

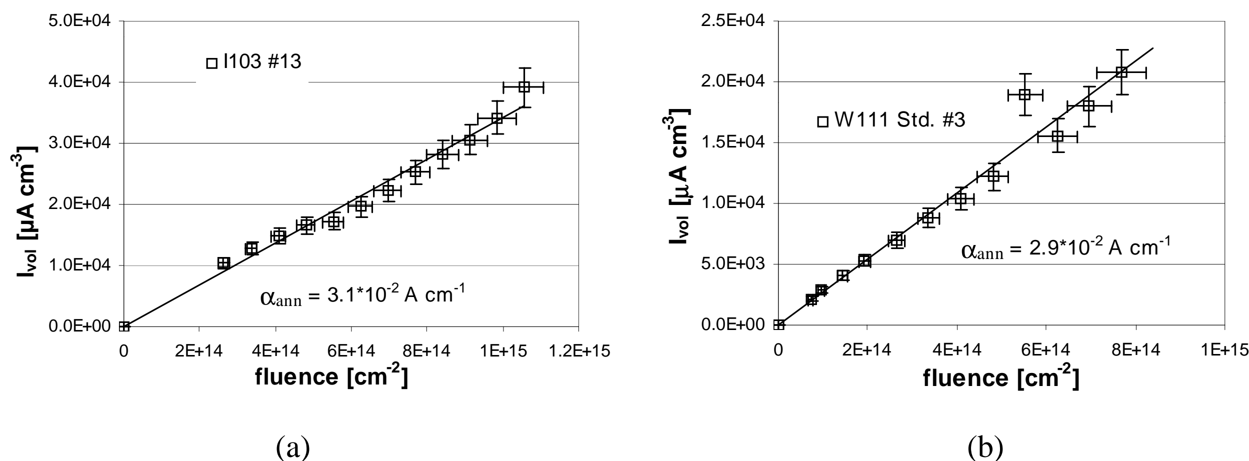


(a) (b)

Fig. 6.32 *$I_{vol}$ as a function of fluence for planar diodes made from low resistivity (a) tin enriched (#13) and (b) standard (#3) FZ wafers. The reverse current has been annealed to 10 days equivalent at room temperature.*

Figure 6.33 shows the reverse current as a function of the fluence for standard (#5), jet-oxygenated (#12) and carbonated (#7) planar diodes irradiated in June '98. $\alpha_{ann}$ is $(2.9 \pm 0.3)\cdot 10^{-17}$ A cm$^{-1}$ for all the diodes.

Figure 6.34 shows the reverse current as a function of the fluence for two planar diodes made from MACOM material (#14), irradiated in June '98. $\alpha_{ann}$ is $(3.1 \pm 0.3)\cdot10^{-17}$ A cm$^{-1}$ for the two diodes.

The parameters obtained from the neutron irradiation data are summarised in Table 6.2.

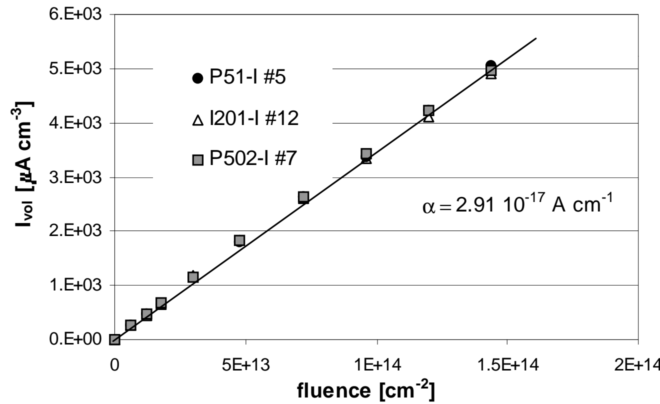


Fig. 6.33 *$I_{vol}$ as a function of fluence for planar diodes made from standard (#5), jet-oxygenated (#12) and carbonated (#7) materials.*

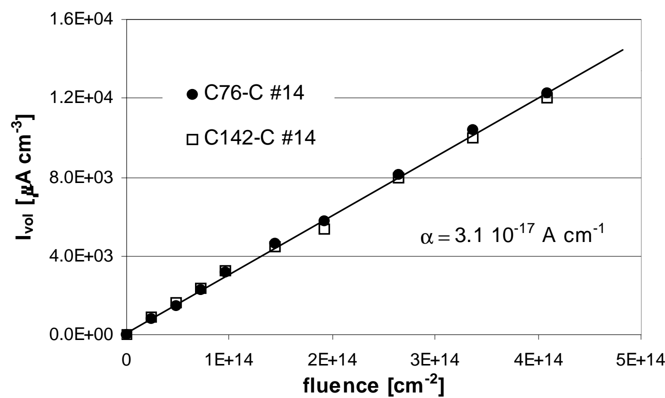


Fig. 6.34 *$I_{vol}$ as a function of fluence for planar diodes made from similar epitaxial wafers* (#14).

## 6.4 Charge collection efficiency as a function of the fluence

The influence of the impurities introduced in silicon on the detection properties of silicon detectors was tested before irradiation. Oxygen or tin concentration up to the introduced levels

does not affect the charge collection properties: and the same charge collection is obtained, before irradiation, by standard and impurity enriched materials.

The charge collection efficiency is found to decrease as a function of fluence. Figure 6.35 shows the typical behaviour of CCE versus 24 GeV/c proton fluence for planar diodes made from materials #2, #5 and #6.

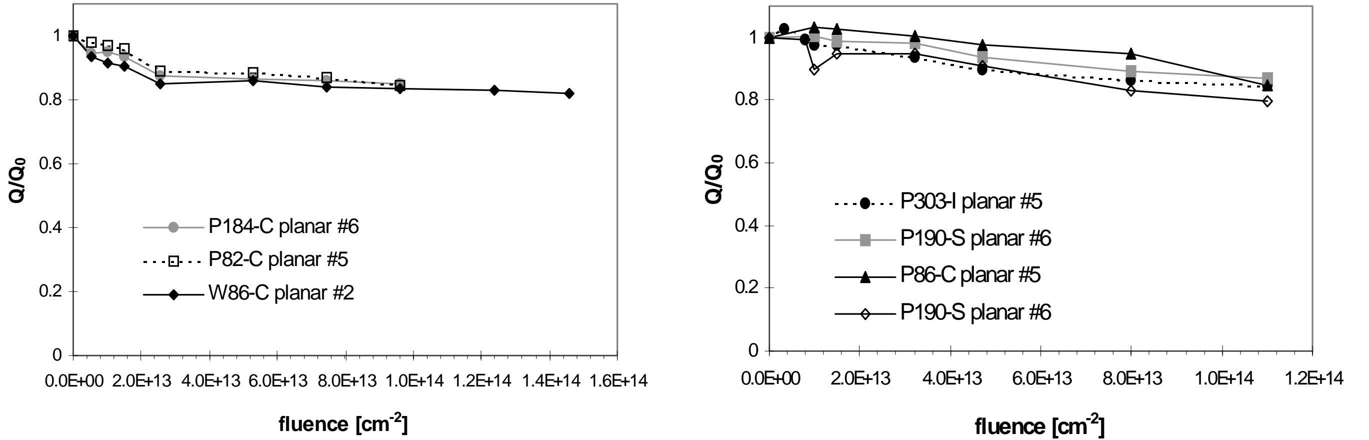


Fig. 6.35 *Charge collection efficiency versus proton fluence for planar diodes made from Standard (#2, #5) and weakly oxygenated (#6) materials.*

## 6.5 Discussion

Tables 6.1 and 6.2 summarise the radiation hardness parameters extracted from the analyses of the proton and neutron irradiation data: $\alpha$, the damage constant of the reverse current, $\beta$, the introduction rate of acceptor-like defects, $g_y$, the amplitude the reverse annealing and $\Phi_{inv}/N_{eff}(0)$, the inversion fluence normalised to the effective impurity concentration before irradiation. These constants are defined in § 3.2. Higher $\Phi_{inv}/N_{eff}(0)$ and lower $\alpha$, $\beta$ and $g_y$ indicate a better radiation tolerance of a specific material. The standard silicon parameters are obtained for planar diodes processed from material #5. The tables present the parameters as calculated from the fluence of the specific radiation (24 GeV/c protons or Triga reactor neutron spectrum) and also as corrected to the equivalent fluence of 1 MeV neutrons, $\Phi_{1MeV}$. The correction is performed according to:

$$\Phi_{1MeV} = k\Phi_{meas.}$$

where $k$ is the hardness correction factor and $\Phi_{meas}$ is the measured fluence of the specific

radiation. The correction factors used are 0.51 and 0.76 for the 24 GeV/c protons and the reactor neutrons respectively [4.17].

### Proton irradiations

| Material | Diode type | 24 GeV/c protons | | | | 1 MeV neutron equivalent | | | |
|---|---|---|---|---|---|---|---|---|---|
| | | $\alpha$ A cm$^{-1}$ | $\beta$ $10^{-2}$ cm$^{-1}$ | $g_y$ $10^{-2}$ cm$^{-1}$ | $\Phi_{inv}/N_{eff}(0)$ cm | $\alpha$ A cm$^{-1}$ | $\beta$ $10^{-2}$ cm$^{-1}$ | $g_y$ $10^{-2}$ cm$^{-1}$ | $\Phi_{inv}/N_{eff}(0)$ cm |
| #1 (FZ std) | planar | $4.5 \cdot 10^{-17}$ | 2.3 | | 20 | $8.8 \cdot 10^{-17}$ | 4.5 | | 10.2 |
| #2 (FZ std) | planar | $4.5 \cdot 10^{-17}$ | 3 | | 20 | $8.8 \cdot 10^{-17}$ | 5.9 | | 10.2 |
| #4 (FZ std) | planar | $5 \cdot 10^{-17}$ | 1.8 | | 21 | $9.8 \cdot 10^{-17}$ | 3.5 | | 10.7 |
| #5 (FZ std) | planar | $5 \cdot 10^{-17}$ | 2. – 2.1 | 2.8 – 3.5 | 17 | $9.8 \cdot 10^{-17}$ | 3.9-4.1 | 5.5-6.9 | 8.7 |
| #6 (FZ – O) | planar | $5 \cdot 10^{-17}$ | 2. – 2.3 | 2.8 – 3.5 | 18 | $9.8 \cdot 10^{-17}$ | 3.9-4.5 | 5.5-6.9 | 9.2 |
| #5 (FZ std) | mesa | | 1.1 | 2.1 – 2.3 | 27 | | 2.16 | 4.1-4.5 | 13.8 |
| #6 (FZ – O) | mesa | | 1.2 | 2.1 – 2.3 | 32 | | 2.35 | 4.1-4.5 | 16.3 |
| #16 (Epi.) | planar | | 2.6 | 4.4 | 18 | | 5.1 | 8.6 | 9.2 |
| #17 (Epi.) | planar | $4.8 \cdot 10^{-17}$ | 2.6 | 4.4 | 17 | $9.4 \cdot 10^{-17}$ | 5.1 | 8.6 | 8.7 |
| #18 (Epi.) | planar | $4.5 \cdot 10^{-17}$ | 2.2 | 4.5 | 12 | $8.8 \cdot 10^{-17}$ | 4.3 | 8.8 | 6.1 |
| #19 (Epi.) | planar | $4.8 \cdot 10^{-17}$ | 2.8 | 5.9 | 20 | $9.4 \cdot 10^{-17}$ | 5.5 | 11.6 | 10.2 |
| #16 (Epi.) | mesa | | 1.1 | 3.8 | 30 | | 2.16 | 7.4 | 15.3 |
| #17 (Epi.) | mesa | | 1.4 | 3.0 | 23 | | 2.7 | 5.9 | 11.7 |
| #18 (Epi.) | mesa | | 1.1 | | 18 | | 2.16 | | 9.18 |
| #20 (Epi.) | mesa | | 1.0 | | | | 2.12 | | |
| #21(Epi.) | mesa | | 1.0 | | | | 2.12 | | |
| #22 (Epi.) | mesa | | 1.0 | | | | 2.12 | | |

Table 6.1 *Radiation hardness parameters extracted from the proton irradiation data.*

The set of diodes irradiated with protons (Table 6.1) explored the range of resistivities from 1.5 (#1) to 7.0 kΩ cm (#4) and O concentrations from < $2 \cdot 10^{15}$ (#5) to $4.5 \cdot 10^{16}$ cm$^{-3}$ (#16). The table also shows the results for planar and mesa processed diodes.

Very little differences are found between planar diodes made from different materials, irrespectively of the impurity contents (O and C), the starting resistivity and the wafer

fabrication technique (epitaxial or FZ). The $\alpha$ values range from 4.5 to $5 \cdot 10^{-17}$ A cm$^{-1}$. The values of $\beta$, of $\Phi_{inv}/N_{eff}(0)$ and of $g_y$ are compared in Fig. 6.36.

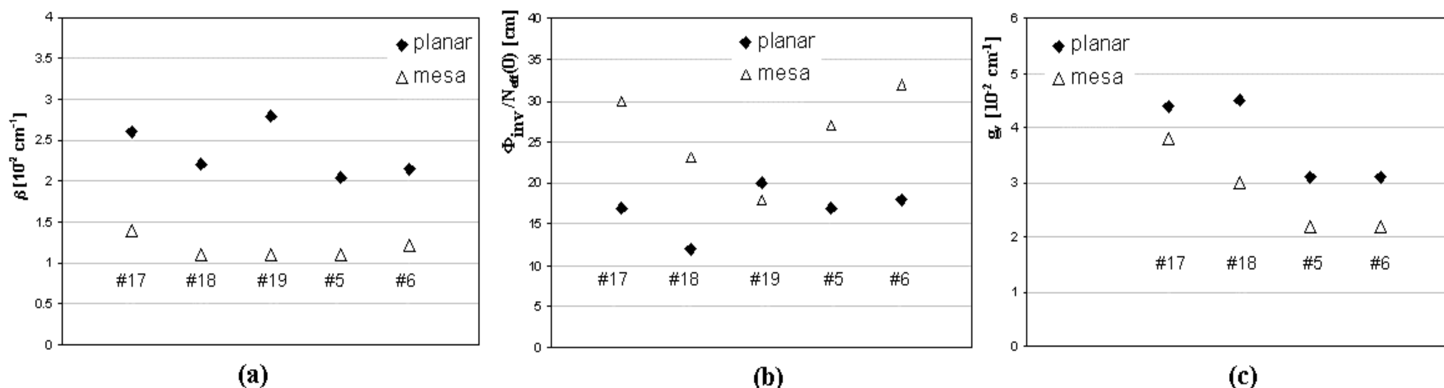


Fig. 6.36 *Comparison between (a)$\beta$ values, (b) $\Phi_{inv}/N_{eff}(0)$ and (c) $g_y$ for various sets of mesa and planar diodes made from a similar material and irradiated with protons (labels # refer to Table 6.1).*

The radiation hardness parameters are systematically better for mesa diodes than those obtained for planar diodes made from a similar material. Especially $\beta$'s are about a factor 2 lower for mesa detectors.

The improvement exhibited by mesa diodes must be related to the diode processing technique. The mesa process induces higher O and C concentrations (at least up to a depth of 60 µm) and high levels of P and B, as evidenced by SIMS measurements.

## Neutron irradiations

Table 6.2(a) shows the radiation hardness parameters for diodes irradiated with neutrons and measured between 30 to 60 minutes after irradiation. Figure 6.37(a) shows the values of $\beta$ for the various materials compared in this group. No noticeable differences are observed between these diodes. In particular, $\beta$ and $\alpha$ values for diodes with diffused oxygen (#8, #9 and #10) are similar to the values of the standard material. The epitaxial material #15 exhibits a slightly better $\beta$ and a worse value of $\alpha$. The NTD silicon diode has the highest $\beta$ between all the tested materials.

| Material | Diode type | Triga reactor neutrons | | | | 1 MeV neutron equivalent | | | |
|---|---|---|---|---|---|---|---|---|---|
| | | $\alpha$ A cm$^{-1}$ | $\beta$ $10^{-2}$ cm$^{-1}$ | $g_y$ $10^{-2}$ cm$^{-1}$ | $\Phi_{inv}/N_{eff}(0)$ cm | $\alpha$ A cm$^{-1}$ | $\beta$ $10^{-2}$ cm$^{-1}$ | $g_y$ $10^{-2}$ cm$^{-1}$ | $\Phi_{inv}/N_{eff}(0)$ cm |
| #5 (FZ std) | planar | $5.9\cdot10^{-17}$ | 3 | 3.0 | 10 | $7.9\cdot10^{-17}$ | 4 | 4.0 | 13.3 |
| #8 (FZ – O) | planar | $6.0\cdot10^{-17}$ | 2.8 | | 9.4 | $8.0\cdot10^{-17}$ | 3.7 | | 12.7 |
| #9 (FZ – O) | planar | $6.1\cdot10^{-17}$ | 2.9 | | 9.5 | $8.1\cdot10^{-17}$ | 3.9 | | 12.5 |
| #10 (FZ – O) | planar | $5.9\cdot10^{-17}$ | 3.1 | | 10.5 | $7.9\cdot10^{-17}$ | 4.1 | | 14 |
| #11 (FZ-O) | planar | | | 4.29 | | | | 5.72 | |
| #15 (Epi.) | planar | 6.5 - 6.7 $\cdot10^{-17}$ | 2.4-2.5 | | 9 | 8.7-8.9 $\cdot10^{-17}$ | 3.2-3.3 | | 6.8 |
| #23 (NTD) | planar | | 3.8 | | 11 | | 5.1 | | 14.7 |

(a)

| Material | Diode type | Triga reactor neutrons (ann.) | | | 1 MeV neutron equivalent (ann.) | | |
|---|---|---|---|---|---|---|---|
| | | $\alpha_{ann}$ A cm$^{-1}$ | $\beta_{ann}$ $10^{-2}$ cm$^{-1}$ | $\Phi_{inv}/N_{eff}(0)$ cm | $\alpha_{ann}$ A cm$^{-1}$ | $\beta_{ann}$ $10^{-2}$ cm$^{-1}$ | $\Phi_{inv}/N_{eff}(0)$ cm |
| #3 (FZ std) | planar | $2.9\cdot10^{-17}$ | 1.2-1.3 | 26-30 | $3.6\cdot10^{-17}$ | 1.6-1.7 | 19.5-22.5 |
| #5 (FZ std) | planar | $2.9\cdot10^{-17}$ | 2.1 | 31 | $3.9\cdot10^{-17}$ | 2.8 | 23.2 |
| #7 (FZ-C) | planar | $2.9\cdot10^{-17}$ | 2.3 | 27 | $3.9\cdot10^{-17}$ | 3.1 | 20.3 |
| #11 (FZ-O) | planar | $3.0\cdot10^{-17}$ | 1.8 | 34 | $4.0\cdot10^{-17}$ | 2.4 | 25.5 |
| #12 (FZ-O) | planar | $3.1\cdot10^{-17}$ | 2.5 | 27 | $3.9\cdot10^{-17}$ | 3.3 | 20.3 |
| #13 (FZ-Sn) | planar | $3.4\cdot10^{-17}$ | 1.6 | 26 | $4.5\cdot10^{-17}$ | 2.1 | 19.5 |
| #14 (Epi.) | planar | $3.2\cdot10^{-17}$ | 0.72-0.76 | 22 | $4.9\cdot10^{-17}$ | 0.96-1 | 16.5 |

(b)

Table 6.2 *Radiation hardness parameters extracted from the neutron irradiation data: measurements performed (a)30-60' after irradiation and (b) after 4' at 80 °C.*

Table 6.2(b) shows the radiation hardness parameters for diodes irradiated with neutrons and measured after an annealing step of 4' at 80 °C. Figure 6.37(b) shows a comparison between the values of $\beta$ for various materials. No effect of the high O concentration on the value of $\beta$ is observed for the material #12 compared to the standard. A slight improvement is observed for the oxygenated material #11. Better results in term of $\beta$ are exhibited by standard materials #3, tin enriched material # 13 and mainly by epitaxial material #14.

Material #3 is a low resistivity FZ silicon. The amelioration of the radiation tolerance shown by

this material is in a certain sense surprising. No particular difference between this material and standard FZ silicon is known. A dependence of the radiation hardness parameters on the resistivity was envisaged [6.2], but no correlation is found in our data, as shown by Fig. 6.38, where $\beta$'s are plotted versus the resistivity for various neutron irradiated diodes.

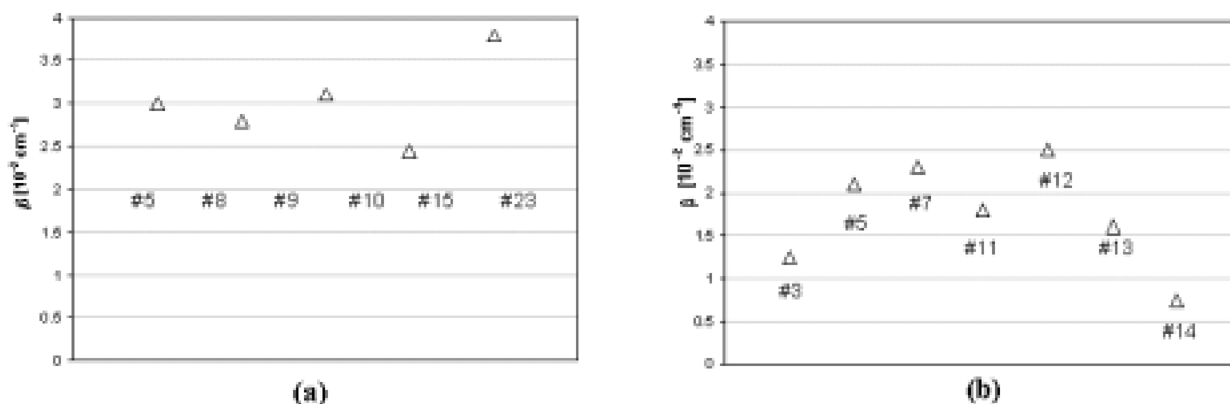


Fig. 6.37 *Comparison between $\beta$ values for neutron irradiated diodes made from various materials. Measurements performed (a) after 30-60 minutes irradiation and (b) after an annealing step of 4' at 80 °C. The labels # refer to Table 6.2.*

The tin enriched material shows a slight improvement of the radiation tolerance compared to the standard silicon. Higher Sn concentrations are required to have a clean signature of its role for the radiation hardening of silicon.

The epitaxial 100 µm silicon produced by MACOM (#14) shows the best radiation tolerance, in term of $\beta$, between all the tested silicon materials, as shown by Fig. 6.37.

The behaviours of the reverse current as a function of fluence are similar for all the measured diodes. The detectors that have better $\beta$'s exhibit no sensitive improvement of $\alpha$. The $\alpha$ values for the epitaxial material #14 are even worse than the ones for the standard silicon.

The generation centres responsible for the current can be either donors or acceptors. The hadron irradiation creates a majority of acceptor-like defects. Nevertheless, it is likely that donor-like defects are created at the same time than the dominant acceptors. A different ratio between acceptor and donor defects could explain the difference found for the $\beta$ parameters of different materials, still maintaining a comparable density of the reverse leakage current.

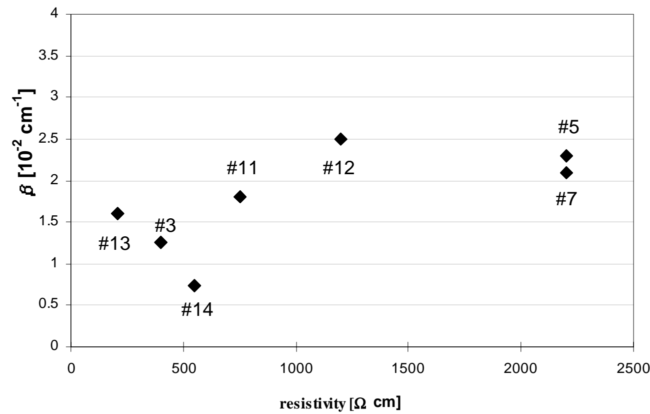


Fig. 6.38 *β versus resistivity for neutron irradiated diodes made from various materials.*

The data presented above permit to clarify some point that has been investigated for long time in the field of the radiation hardness of silicon detectors.

The role of oxygen, proposed by many workers as a possible candidate for the radiation tolerance improvement of silicon, has been studied over a wide range of concentrations: from $2\cdot10^{15}$ up to $2.5\cdot10^{17}$ $cm^{-3}$. No systematic dependence of the radiation tolerance on the O concentration is evidenced.

It was suggested [1.8] a possible influence of C, which could form C-O complexes and reduce the effectiveness of O as vacancy sink, but also no dependence of the radiation hardness parameters on the ratio of oxygen to carbon concentration is found.

Oxygen was found to increase the radiation tolerance of silicon detectors in the case of gamma (from $^{60}Co$) irradiation [3.10]. The inefficacity of O to improve the radiation hardness of silicon in the case of hadron irradiation should be related to the defects forming in terminal clusters. The local density of $V_2$ defects in clusters can be up to $10^{20}$ $cm^{-3}$. If the dominant complexes responsible for the change of the electrical properties of silicon react into the cluster volume, the concentration of impurities acting as vacancy sinks has to be comparable to this number. The oxygen and tin concentrations introduced in silicon up to now are order of magnitude smaller than this value.

The suitable impurity levels should therefore approach $10^{20}$ at. $cm^{-3}$. This value exceeds the solubility limit of oxygen and carbon in silicon.

Moreover, the impurities introduced in such a large concentration must be electrically inactive in order to avoid the drop of the resistivity. The drop of the resistivity from an initial value of

500 to ≈ 200 Ω cm after the Sn enrichment seems to prove that tin is a donor in silicon. In that case, higher tin concentrations would result in resistivity value too low for detector applications.

The deliberate introductions of impurities in FZ silicon do not exhibit satisfactory results in term of radiation hardening. Nevertheless some materials shows improved behaviours, such as the standard FZ #3 and, particularly, the epitaxial material #14.

The improvement shown by mesa diodes could be related to the high B and P concentrations as measured by SIMS. The usual annealing process did not activate the P and therefore it could be present in a complex stable up to 800 °C. However, no information is available about the existence of such a complex and its interaction properties with radiation induced defects.

The reasons for the improvement exhibited by the FZ material #3 and, in a larger extent, by the MACOM epitaxial material #14 are not understood, but they are probably related to the fabrication process.

The epitaxial material contains O and C, but their role should be excluded in view of the experimental results obtained from oxygenated and carbonated (#7) FZ materials which do not exhibit any significant improvement. Furthermore, this amelioration is not simply related to the epitaxial growth technique: other epitaxial materials grown by ITME and by the same MACOM Company do not show a noticeable improvement. A possible candidate is hydrogen, which is present during several steps of the manufacturing processes. The high mobility of hydrogen in silicon could explain the high concentration required in order to affect the formation of the final defects.

A close collaboration with the silicon manufacturer (MACOM) for the analysis of the production details is on the way to find out the ingredients that lead to this promising result.